Université Pierre et Marie Curie
Faculté de Chimie

Rapport de stage M2 Mol

Manipulating Min Protein Patterns

Markus Mittnenzweig
markus.mittnenzweig@etu.upmc.fr

Advisors:
Prof. Dr. Petra Schwille
Prof. Dr. Damien Baigl

Submitted 06/20/2014

Contents

1 Introduction

Cells are the basis of life being the smallest unit that all living things have in common. To ensure its survival every cell has to reliably perform certain tasks such as DNA replication or cell division. The analysis of such cellular processes remains - despite great advances - notoriously difficult. This is in part due to the complexity of biological systems, i.e. that a cellular process such as the cell cycle can involve more than 100 proteins.

Bacterial cells are much smaller and less complex than their eukaryotic counterparts. It was longtime believed that they lack a cytoskeleton and that the inside of bacteria is a homogeneous mixture of its components [1, 2]. However the last two decades have completely changed this view. Nowadays it is clear that bacteria have a cytoskeleton that controls in particular shape and division of bacterial cells [3]. One of its most prominent representatives is FtsZ. At some point during the cell cycle it forms a ring structure on the membrane which determines the future position of cell division. It has been shown that bacteria can localize proteins and establish intracellular concentration gradients that help structuring the space [4, 5, 6]. The identified proteins are involved in processes such as the positioning of the cell division plane and spatial separation of organelles such as sister chromosomes, plasmids or carboxysomes [7, 8].

All these examples stand for the emergence of molecular self-organizing protein systems in bacteria. Self-organization has been observed in several other biological and chemical systems. Its study goes back to the work of Turing [9] and Nicolis and Prigogine [10]. It has been studied in much detail in the famous Belousov-Zhabotinsky reaction. Pattern-forming systems have in particular been found in the field of heterogeneous catalysis where kinetic oscillations have been observed in more than 20 chemical surface reactions [11, 12]. Fig. 1.1 shows spiral surface waves in the CO oxidation on a Pt(110) support and spiral waves of the Min protein systems that form *in vitro* on lipid bilayers. The analogy of the basic underlying reaction mechanism is quite appealing. Both systems have only two reactants and the patterns form on a two-dimensional support.

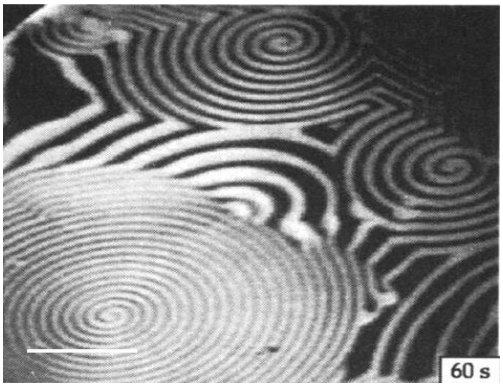

$$CO + * \longrightarrow CO*$$

$$O_2 + * \longrightarrow 2\,O*$$

$$CO* + O* \longrightarrow CO_2 + 2\,*$$

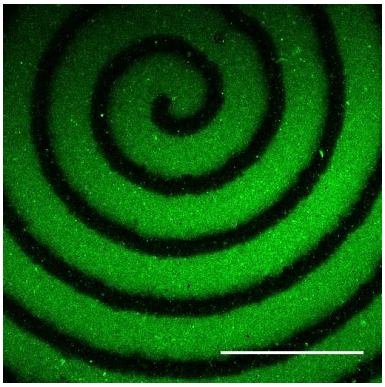

$$MinD\text{-}ATP + * \longrightarrow MinD\text{-}ATP*$$

$$MinE + MinD\text{-}ATP* \longrightarrow MinDE\text{-}ATP*$$

$$MinDE\text{-}ATP* \longrightarrow MinD\text{-}ADP + Pi + MinE*$$

$$MinE* \longrightarrow MinE + *$$

Figure 1.1: The image on the right shows an example of a Min wave with a simplified reaction mechanism of the Min oscillator. The image on the left is taken from [12]. It shows a PEEM image of the Pt(110) surface in the CO oxidation reaction and on the bottom the reaction mechanism of the CO oxidation. The * stands for positions on the membrane or Pt surface respectively. Note the principal similarities in the reaction mechanisms. The substrates bind to the 2D support, react and then debind again. The scale bar is $100\,\mu m$ in both images.

The aforementioned Min protein system is a fascinating example out of the group of self-organizing phenomena in bacteria. It consists of the three proteins MinC, MinD and MinE which spontaneously oscillate on the cell membrane from one cell pole to the other [13, 14, 15]. It has been shown that only MinD and MinE are necessary for the spatial oscillations whereas MinC has an affinity for MinD and therefore just follows the MinD wave. It is needed to couple the MinDE oscillator to FtsZ by simultaneously inhibiting FtsZ polymerization. The Min oscillations produce a time averaged spatial concentration gradient of MinC (see Fig. 2.2 (a)) with the average concentration of MinC being lowest at the midcell plane and highest at the cell poles. Several studies suggest that this concentration gradient of MinC prevents the formation of FtsZ rings at the cell poles[16, 17, 18].

It is remarkable that only two proteins and a membrane are required to produce spatial oscillations on the micrometer scale. This makes the Min system also attractive as a component for the construction of an artificial minimal cell [19, 20]. One could also imagine to use synthetic analogs that interact through the mechanism with each other. In view of this synthetic approach it is desirable to understand the design principles of the Min protein systems. A major progress in understanding the underlying mechanism was made by showing that MinD and MinE self-organize *in vitro* on lipid bilayers into concentration surface waves[21].

Until now techniques are limited to manipulate Min protein patterns *in vitro*. We have therefore developed a membrane clad flow cell using a 3D printing method. It permits control and rapid change of solution parameters such as protein concentrations or viscosity. Lipid bilayers inside the flow cell are mobile and Min protein waves can be reconstituted.

It is challenging to acquire high resolution images of dynamic protein structures since super resolution techniques such as PALM or STORM offer only low temporal resolution. We could show that one can in principle circumvent this problem in the case of Min waves. Using our flow cell setup the propagation of Min waves could be stopped by exchanging the aqueous buffer by oil. By the same technique we could cover water-filled microcompartments with oil. These microcompartments very recently used to reconstitute *in vitro* Min oscillations

and the new setup could provide better time stability.

The work is structured as follows: The next section gives an introduction to the biological context of the Min protein system. We then present and discuss our findings in details. The experimental techniques are explained at the end of this work.

2 Regulation of cell division by the Min system

2.1 Bacterial cell division

Most bacteria grow and divide by a process called binary fission. After reaching a certain mass and length and replicating their DNA the bacteria divide into nearly two identical daughter cells [22, 23, 24]. The cell division process can be divided into a few steps: (i) The cell has to select first where to divide. Many bacteria, including *Escherichia coli*, *Bacillus subtilis* or *Caulobacter cresentus* seem to apply intracellular protein gradients to determine the position of the division site [5]. (ii) In most bacteria, the next step is the formation of the FtsZ ring at the future division site [22]. The cytoskeletal FtsZ protein is a structural homologue of the eukaryotic tubulin [25]. It oligomerizes into short filaments which can bind to the membrane via intermediate membrane binding proteins such as FtsA. At some point during the bacterial cell cycle, these short membrane bound FtsZ filaments then assemble into a clearly visible ring at the midcell position, the FtsZ ring [26, 27, 28, 29, 22] (see Fig. 2.1). (iii) The FtsZ ring works as a scaffold. As soon as it has formed further proteins attach to it and self-assemble into a macromolecular complex, the divisome which synthesizes the outer cell wall consisting of peptidoglycans. After having assembled the divisome the Z ring contracts within a few minutes and the cell divides into two daughter cells [29]. This is a simplified version of bacterial cell division. It has to be coordinated with other cellular processes, in particular with chromosome replication and segregation. Most mechanistic details of this regulation are still unkown.

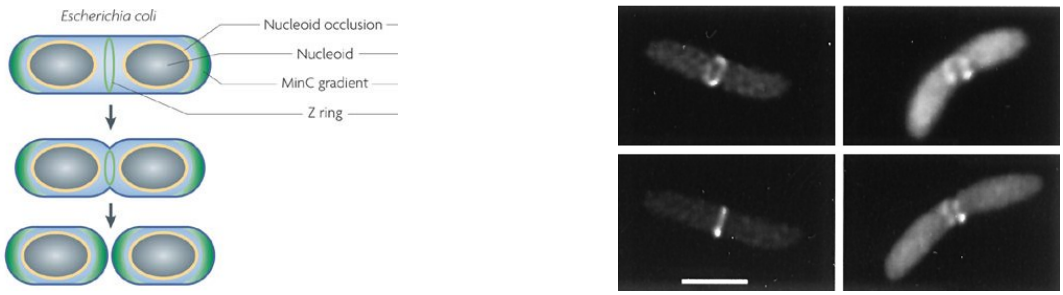

Figure 2.1: Bacterial cell division: Rod-shaped bacteria such as E. coli divide at the midcell position. Cell division at the cell poles is prevented through a high concentration of MinC. The right image (taken from [30]) shows the Z ring in E. coli cells (FtsZ-GFP was used as fluorophore). The scale bar is $1\,\mu m$. The figure on the left is taken from [29].

2.2 The Min system as an example of a spatial oscillator

In rod shaped bacteria such as *E. coli,* the FtsZ ring always forms at the midcell plane with only low spatial variability [31]. In *E. coli* the Min protein system controls the position of the FtsZ ring. It consists of the proteins MinC, MinD and MinE which spontaneously oscillate on the membrane of the cell from one cell pole to the other with an oscillation period of about 40s [13, 14, 15].

The name of the Min proteins originates from the anuclear minicells that form f one of the three Min proteins is not expressed. Oscillations with several nodes have been observed in long filamentous cells as well as in long *in vitro* microcompartments [33]. Theoretical simulations also reproduced oscillations with several nodes [34, 35]. These findings suggest that the Min oscillator has an intrinsic wavelength. Surprisingly the *in vivo* and *in vitro* wavelengths differ roughly by a factor of ten[36]. The proteins MinD and MinE are necessary and sufficient for the oscillations whereas MinC couples the spatial oscillations to the FtsZ system. MinC forms a homodimer that contains a MinD-binding domain and a FtsZ interacting domain that inhibits Z ring assembly [17, 16].

MinD is a rather large membrane ATPase (29kDa) that belongs to the WACA family (Walker A cytoskeletal ATPases) of APTases [37]. Most of them, including MinD, form dimers in solution in the presence of ATP. Several members of this

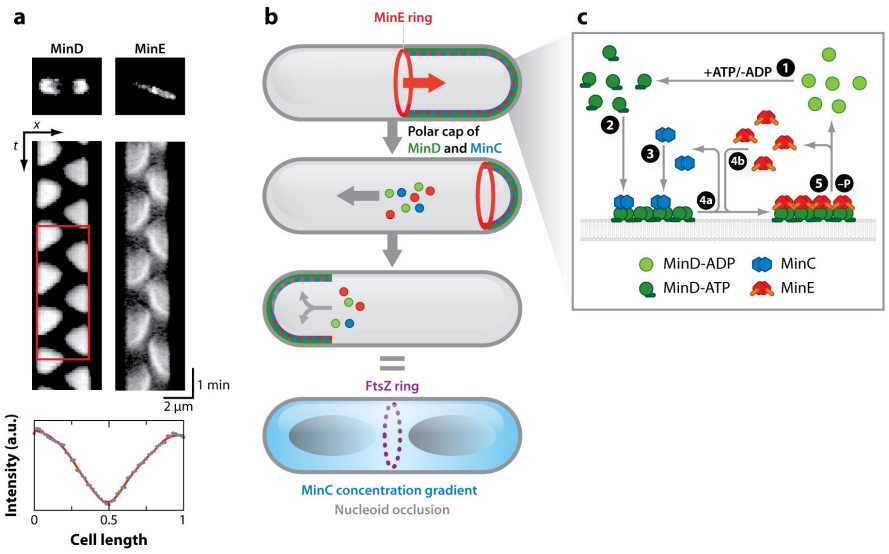

Figure 2.2: (figure taken from [32]) (a) In vivo oscillations of the Min system Top: space time plot (kymograph) of MinD and MinE. In the kymograph of MinE the characteristic MinE ring can be seen. Bottom: a time average of the MinD concentration of the red rectangle is shown. One sees that the concentration of MinD is significantly lower at the midcell plane than at the cell poles. (b) and (c) show the oscillatory reaction cycle of MinD and MinE.

family were shown to be involved in the spatial organisation of bacteria, such as ParA which is necessary for plasmid segregation or the Soj protein that helps segregating the chromosomes.

MinD is the only member of that family that also has an amphiphatic helix enabling it to bind to membranes. While its membrane affinity is very low in the ADP state, it is much augmented in the presence of ATP [38, 1, 39, 40] which is most probably due to the ATP-dependent dimerization of MinD. Moreover, *in vitro* experiments showed that MinD membrane binding does not follow a simple Langmuir adsorption isotherme but can be described by a Hill coefficient of 2 [41, 42]. This means that MinD binds cooperatively to membranes, i.e. the binding of MinD to the membrane is favored if other MinD molecules are already attached to the membrane. It is not known if this cooperativity stems from a dimerization or oligomerization of the MinD dimers on the membrane or if it is just due to some weak attractive interaction between Min proteins. *In vitro* experiments have shown that MinD can in principle form polymers at high protein concentrations and in the presence of ATP and phospholipid vesicles [43]. However, it is not known if oligomerization of MinD is also significant at physiological concentrations.

The basal ATPase activity of MinD in solution is very low. It is only stimulated (by a ten-fold) in the presence of a lipid membrane and MinE [43]. MinE is a small 88-residue that forms a homodimer [44] and binds to MinD on the lipid membrane. MinE also has a short membrane targeting sequence as well which might amplify its affinity for membrane-bound MinD. The complex formation of MinD and MinE in turn stimulates the ATP hydrolysis of MinD-ATP. Once hydrolyzed, MinD-ADP has a reduced affinity for the lipid bilayer and detaches from the membrane. However, *in vitro* experiments have shown that MinE has longer membrane residence times than MinD [44], i.e. it stays on the membrane after the detachment of MinD-ADP [44] and can bind to another molecule of MinD-ATP. This effect was called *persistent binding* and might explain the formation of MinE rings, i.e. that a front of high MinE concentration forms *in vivo* and seems to processively clear the membrane of MinD. The persistent membrane binding of

MinE is probably due to the short membrane targeting sequence that MinE homodimers contain [45]. After MinD-ADP detaches from the membrane, the ADP molecule is exchanged in solution by ATP and the biochemical reaction cycle of MinD dimerization, membrane binding and ATP hydrolysis restarts. Fig. 1.1 and 2.2 (c) summarize the biochemical reactions again. In conclusion, the *in vivo* Min oscillations are fuelled by a reaction cycle containing ATP hydrolysis. The main sources of nonlinearity are the cooperativity of MinD membrane binding and the persistent binding of MinE both ensuring that the reaction cycle oscillates and does not equilibrate.

In vitro reconstitution The biochemical mechanism shows that the Min system exhibits temporal kinetic oscillations. But it does not explain how the system can produce spatial oscillations. Therefore, the reaction needs to be coupled with diffusion. *In vitro* reconstitution studies of the Min system could elucidate this question. When adding MinD, MinE and ATP to a supported lipid bilayer of E. coli lipids, the proteins spontaneously self-organize into travelling surface waves on the lipid bilayer as shown in Fig. 2.3. The profiles of MinD and MinE show some characteristic properties. The convex shape of the MinD profile is probably due to the cooperative membrane binding of MinD. The second important point is the sharp peak of MinE at the end of the wave, which is even behind the MinD maximum. This peak resembles the *in vivo* MinE ring and they both seem to clear the membrane of bound MinD. So far it is not clear how these MinE fronts form. One proposed idea is that MinE accumulates at the end of the wave due to membrane diffusion and persistent membrane binding [44]. However, no theoretical simulation reproduced the MinE ring so far, which indicates that some mechanistic detail might still be missing. Besides Min waves, Min oscillations could also be reconstituted *in vitro* by restricting the bulk solution to micrometer-sized sample volumes. To achieve this the Min system was reconstituted on lipid bilayers in small microcompartments as schematically shown in Fig. 2.3.

The main difference between the *in vivo* and *in vitro* situation lies in the different length scale and propagation speed of the wave fronts. The *in vivo*

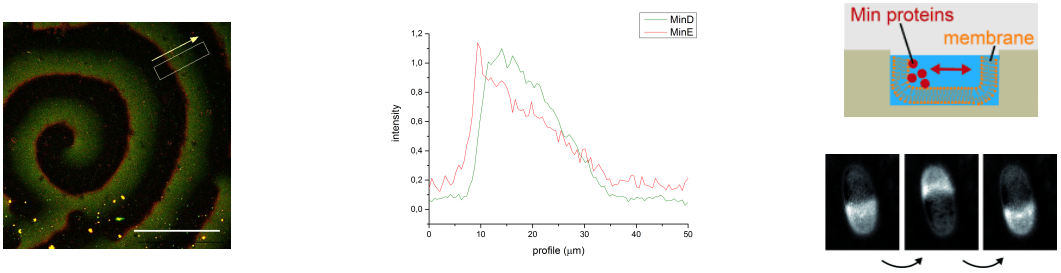

Figure 2.3: The left image shows an example of a Min wave. MinD is coloured in green and MinE in red and the corresponding wave profiles of MinD and MinE are displayed in the center. The image on the right shows reconstituted *in vitro* oscillations of MinD and MinE in water-filled microcompartments and is taken from Zieske and Schwille [33]. The scale bar on the left is $100\,\mu m$.

wavelength does not exceed $5\mu m$ and the MinE front propagates with a velocity of around $0.05\,\mu m \cdot s^{-1}$ whereas the *in vitro* wavelength typically lies in the range of 40 to $100\,\mu m$ with the velocity ranging from $0.4 - 1.0\,\mu m \cdot s^{-1}$ [36].

3 Results

3.1 Min waves can be reconstituted in a 3D printed flow channel

Until now *in vitro* studies on Min proteins were mostly done using open compartments. These compartments are not well suited to exchange the buffer solution by another one. Therefore we decided to construct a closed reaction chamber that would permit easy solvent exchange. to Using a 3D printer we designed and manufactured a flow channel (Fig. 3.1 on the left). Printing of one flow channel took 30 min. After glueing the channel to a PDMS-covered glass cover slip and attaching silicon tubes to two entrances we obtained a closed flow cell (Fig. 3.1 on the right).

A lipid bilayer consisting of *E. coli* polar lipids and Min proteins could be reconstituted inside the flow cell on the surface of the cover slip (see fig. 2.3 for an example of a wave obtained with the flow cell setup). The detailed protocol is

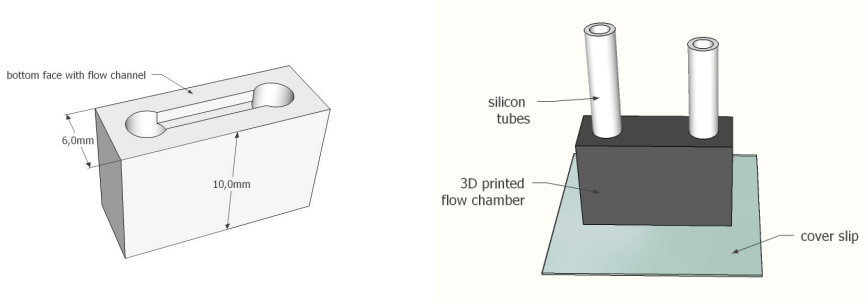

Figure 3.1: The flow cell: On the left we see a model of a flow channel and on the right we see the experimental setup when the channel is glued on a glass cover slip and silicon tubes are attached to the entrances of the flow cell.

described in the methods section. The flow cell construction is flexible. Instead of a PDMS support one could also connect the flow channel with a Mica or glas support and one can easily modify the geometry. We used two syringes to wash the lipid bilayers inside flow cell in order to remove non-fused lipid vesicles from the surface. A clean lipid bilayer was crucial to obtain regular Min waves. The flow channels were reused after each experiment.

3.2 Immobilization of Min patterns

Throughout all experiments we used fluorescence microscopy to image Min waves. We used MinD-GFP as a fluorophore. In all experiments unlabelled MinD was mixed with MinD-GFP in a 3:1 ratio. Min protein patterns are dynamic self-organized structures. So far it was not known if the propagation of the wave fronts can be delayed or stopped. Aiming at stopping the Min protein waves and using our flow cell setup we designed the following experiment: We first produced a PDMS-supported lipid bilayer inside the flow cell (see methods section 5.3) and then incubated it with MinD and MinE in the presence of ATP until regular Min waves had formed. The aqueous buffer was then exchanged by light mineral oil to stop the propagation of the Min waves.

Fig. 3.2 shows the image and profil of a Min wave in the aqueous solution. We acquired a time series and the space time plot (kymograph) of a cross section

of a Min wave (the rectangular area in 3.2 (a)) shows that the Min waves are propagating.

The aqueous solution was then rapidly exchanged (flow rate of $600\mu l/min$) by a solution of apolar light mineral oil. In parts of the flow channel Min proteins were completely washed away from the bilayer. But Min proteins remained on the membrane in the region which is below the entrance tube. Fig. 3.2 (c) shows a Min wave after the exchange to oil. However, the waves do not move anymore as proved by the kymograph in Fig. 3.2 (d). We also compared the intensity profile of the Min proteins before and after the exchange to oil. The fluorescence intensity drops as shown in Fig. 3.2 (e), but the shape of the MinD profile does not change after subtracting the background and normalizing the intensities. This suggests that parts of the Min proteins are washed away by the oil but the percentage of proteins that remain on the membrane does not depend on the position in the wave.

To elucidate if the Min proteins might diffuse on time scales longer than minutes we photobleached a rectangular area inside a MinD wave (see methods section 5.8) . If MinD molecules were mobile and diffuse on the membrane, the fluorescence intensity in the bleached area should recover, at least at the border of the rectangle. However, even after eight days no visible blurring of the rectangular border could be observed as shown in Fig. 3.3. Thus, Min proteins are immobile in oil on the time scale of several days.

We were wondering if the properties of the lipid bilayer were affected by the exchange from aqueous solution to mineral oil. Using a fluorescent membrane dye and doing a FRAP experiment (see methods sectio 5.8) we checked for two samples if the mobility of the lipid changes when replacing the aqueous buffer by oil. As shown in Tab. 1 we could not detect any significant change in the diffusion coefficient of 0.1% ATTO647-DOPE in the lipid bilayer. This would suggest that the lipid bilayer does not change its physical properties and remains at the PDMS-solution interface. On the other hand the lipids of the lipid bilayer are soluble in mineral oil.

In summary we have shown that Min proteins remain on the membrane in

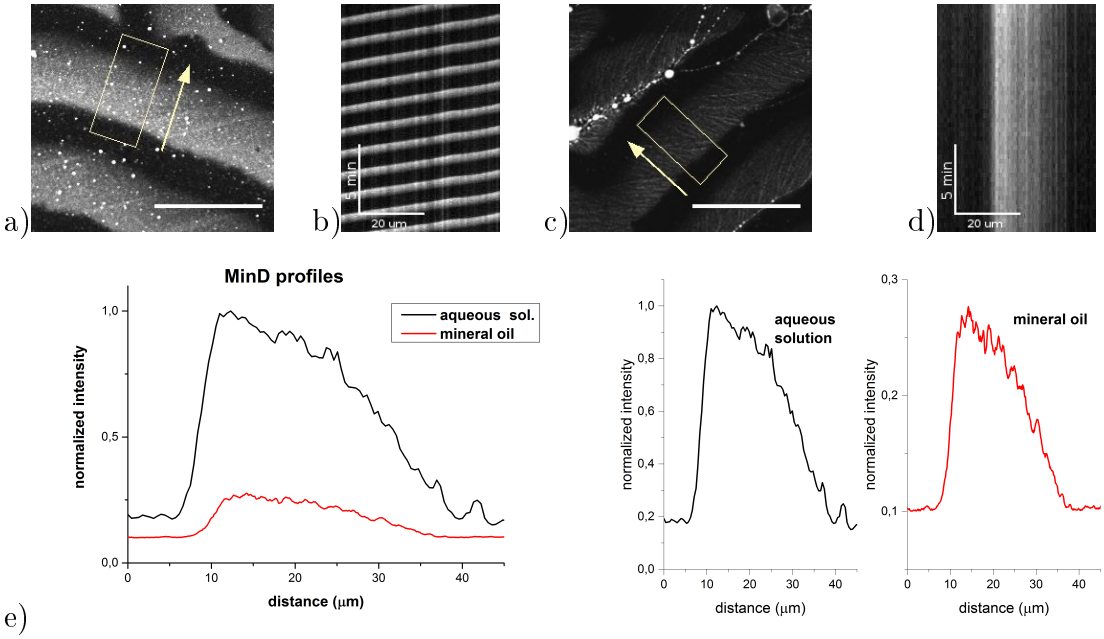

Figure 3.2: On the top we see fluorescence images and kymographs of MinD waves before ((a) and (b)) and after adding oil ((c) and (d)). The kymographs show the space time intensity plots of the yellow boxes. The scale bar is $50\,\mu m$. The bottom diagrams show the MinD profiles in aqueous buffer and in mineral oil. After subtracting the background, the maximal fluorescence intensity in oil drops to 20% of the maximal intensity in the aqueous buffer. The shape of the MinD profile does not change.

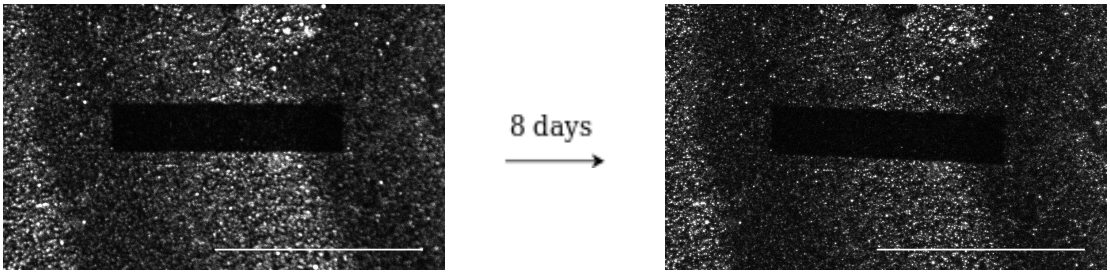

Figure 3.3: Min proteins are immobile in mineral oil. Even after eight days we could not detect any visible recovery of the fluorescence inside the photobleached rectangle. The scale bar is $50\,\mu m$.

diff. coeff. $\left[\frac{\mu m^2}{s}\right]$	1	2
aqu. solution	0.23 ± 0.01	0.21 ± 0.01
oil	0.25 ± 0.02	0.22 ± 0.03

Table 1: Diffusion coefficient of 0.1% Atto647-DOPE in the supported lipid bilayer: for each of the two samples we acquired ten FRAP curves ($5\mu m$ bleaching radius) in aqueous solution and in oil and then calculated the diffusion coefficient from it as described in the methods section 5.8.

parts of the flow cell when exchanging the aqueous buffer by oil. However they do not diffuse anymore on a time scale of several days whereas the mobility of the lipid bilayer does not change. The experiment shows that a rapid change of the solution properties can be a convenient way to delay or immobilize dynamic membrane interacting processes.

3.3 Enclosing microcompartments with mineral oil

Min oscillations were recently reconstituted *in vitro* in water-filled microcompartments [33]. However, the microcompartments are not enclosed and sample volume has a water-air interface (see Fig. 2.3 on the right). Due to this the micrometer-sized sample volumes will be evaporated after a few minutes. Using our flow cell setup we therefore aimed at replacing the water-air interface by a water-oil interface. By adding lipids to the oil one might also create a lipid monolayer at the water-oil interface. As a first step the following experiment was designed:

The flow cell was incubated with an aqueous solution containing a hydrophylic fluorescent dye (shown in green). Using a syringe the aqueous solution was then exchanged by mineral oil containing a lipophilic fluorescent dye (shown in red). Fig. 3.4 shows that the aqueous solution remains in the microcompartments and that it is covered by the oil phase. A major problem was that the oil often flushed away most of the water in the microcompartments. One should overcome these problems by adjusting the flow rate of the oil and using a suitable alignment of the microstructures with respect to the flow direction. The next step would be to reconstitute Min oscillations in the enclosed microcompartments.

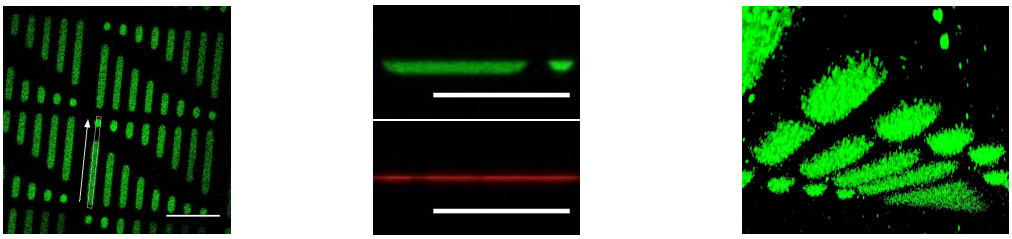

Figure 3.4: Microcompartments: The green color corresponds to the fluorescence intensity of a hydrophylic dye. On the left a 2d view of the microcompartments is shown. In the center the $x-z$ intensity profile along the white arrow in the left image is shown. Green shows the fluorescence intensity of the hydrophylic dye and red the fluorescence intensity of a lipophilic dye that was added to the oil. The profiles show that the aqueous solution remains in the microstructures after the exchange to oil and that it is covered by the oil solution. The image on the right shows a 3D view of the microstructures. The scale bar is $50\,\mu m$ in every image.

3.4 Transition to higher MinE/MinD ratios

As a next step we were interested if we could manipulate the Min waves by controlling certain solution parameters such as protein concentrations or viscosity of the buffer. So far techniques to manipulate *in vitro* patterns are limited. As a first step we therefore tried if we can manipulate Min protein waves by changing the MinE/MinD ratio. It is expected that the *in vitro* wavelength should decrease and that the velocity should increase with increasing the MinE/MinD ratio[21]. The following experiment was done: The MinE concentration in the flow cell was first doubled from $0.75\,\mu M$ to $1.5\,\mu M$ while the MinD concentration remained constant at $0.75\mu M$ (transition 1). In the second step (transition 2) we returned to the initial concentrations of MinD and MinE. Table 2 shows the respective wave velocities before and after each transition. Between transition 1 and transition 2 we waited for approximately one hour. As expected the wave velocity first increases for increasing MinE/MinD and then slows down again when returning to the initial concentrations. After the second transition the velocities do not completely reach the initial level. One reason for could be that there occurs some mixing of the different solutions during the exchange during. But in principle the experiment shows that the reversible switch between different solution conditions

	transition 1		transition 2	$[\mu m/s]$
	before	after	before	after
1	0.29	0.70	0.55	0.39
2	0.34	0.66	0.62	0.39
3	0.31	0.78	0.67	0.57

Table 2: For three sample, we measured the velocities of the Min waves before and after each transition. Transition one corresponds to an increase of the MinE concentration from $0.75\,\mu M$ to $1.5\,\mu M$ and transition two to a decrease from $1.5\,\mu M$ to $0.75\mu M$. The MinD concentration of $0.75\mu M$ was not changed.

is possible.

The transition to higher MinE concentration

Since we can image the lipid bilayer during the exchange of the solution we could also observe how the Min waves change when increasing the MinE concentration. Fig. 3.5 shows an example of such a transition. A few seconds after the solution exchange, the original wave profile becomes unstable (in 3.5 after $20\,s$) in the sense that new MinE fronts form inside the MinD wave. These MinE fronts separate the back part of the MinD wave from the front part. This type of transition has also been observed, when increasing the viscosity of the solution but leaving the concentrations unchanged (not shown here). It seems to take place in general when the width of the wave fronts decreases. We have also several times observed the variant that the new MinE front forms in the front part of the MinD wave thereby annihilating nearly the whole Min wave. We would expect that this transition always happens when the kinetics change in favor of MinE membrane binding.In general, the observed transition resembles the *in vivo* situation where a MinE front forms at the midcell when the MinE concentration is temporarily increased.

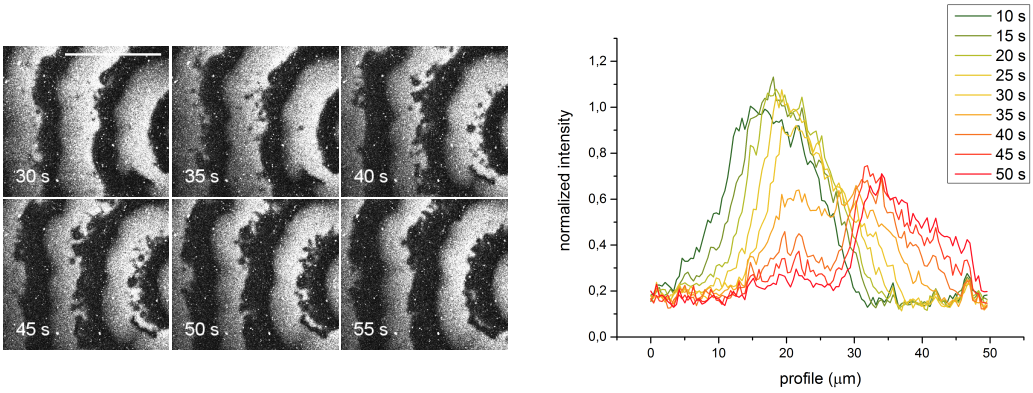

Figure 3.5: Transition to higher MinE concentration: 30 s after the increase of the MinE concentration in the buffer, new MinE fronts form inside the MinD wave that eliminate the back part of the wave. The figure on the right shows the profile of MinD during this transition.

3.5 Chaotic patterns

As was pointed out before the *in vitro* wavelength and velocity is by a factor 10 larger than the *in vivo* wavelength and velocity. It has been suggested that the membrane fluidity and solution viscosity are the main parameters influencing wave length and velocity [36, 32]. We thus performed the following experiment: We exchanged the aqueous buffer by a more viscous solution with the protein concentrations unchanged. The viscosity of the protein buffer was increased by adding the crowding agent ficoll to a final mass percentage of 10%. Ficoll is a polysaccharide that is frequently used as a crowding agent [46]. The results on the change in velocity or wave length were not conclusive so far. For several samples we observed the formation of more complex spatiotemporal patterns as shown in Fig. 3.6. These patterns are probably functional, in the sense that the proteins are not denatured. In the example of 3.6 the chaotic patterns evolved into regular waves again after 2 to 3 h. So far we could not conclude, under which conditions these chaotic patterns form and if they are always transient or if there exists a parameter regime where they are stable for several hours. However it is known that chaotic patterns and chemical turbulence are common phenomena

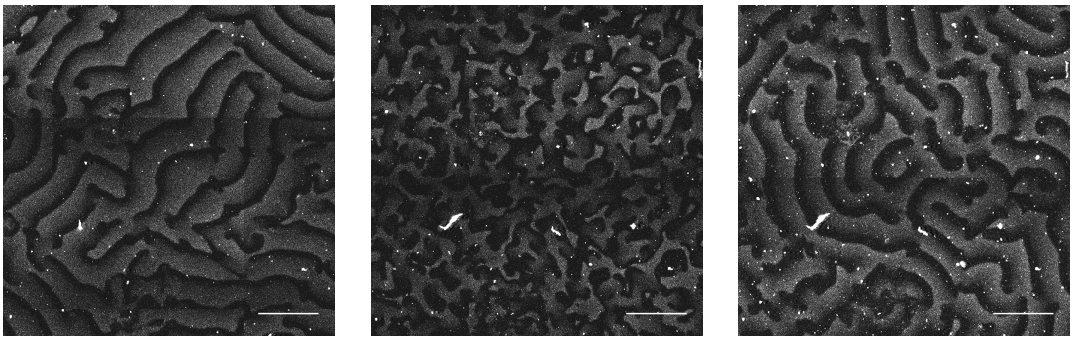

Aqueous buffer | Ficoll 10% after exchange | Ficoll 10% 3h later

Figure 3.6: Transient chaotic patterns: The MinD and MinE concentrations are the same for every image. We started with an aqueous buffer on the left and then increased the viscosity and crowding property of the solution by adding 10 % Ficoll. Switching to 10 % Ficoll gives rise to transient chaotic patterns that disappeared after 2 to 3h. All images show the same region on the membrane. The scale bar is 100 μm.

in chemical reaction diffusion systems [47, 48]. Another problem that made the analysis difficult was the frequent formation of artefacts (not shown here, but reported in [49]) when changing to higher viscosity. It could be that the proteins become less stable due to the addition of the 10% Ficoll and tend to denature.

4 Summary and Outlook

In this work we constructed a 3D printed flow cell and showed that supported lipid bilayers as well as Min protein waves can be reconstituted in it. The flow cell was used to immobilize Min protein patterns by rapid exchange of the aqueous buffer by light mineral oil. It is a promising technique to obtain static images of dynamic membrane interacting systems.

The succesful stopping of the Min waves have laid the basis to investigate Min protein patterns with super resolution techniques (PALM, STORM). Their main requirement, very static samples, is fulfilled by the immobilized Min waves. STORM requires a suitable reducing agent and one would need to adapt the setup to mineral oil as a solvent.

Microcompartments in PDMS were recently used to reconstitute Min oscillations *in vitro* [33]. Combining the flow cell setup with these microfabricated PDMS structures we obtained water-filled microcompartments that are covered by oil. Compared to the experiment in [33] the water-air interface was thus exchanged by a water-oil interphase which provides higher time stability since the water cannot evaporate anymore. The next step would be to reconstitute Min oscillations in these enclosed microcompartments.

By connecting the flow cell to a pump we could acquire live images while simultaneously changing solution parameters. It was shown that it is in principle possible to reversibly switch between two states. And we can also observe how one protein pattern evolves into another one. As an example, we studied the transition to higher MinE concentrations. After increasing the MinE concentration, new MinE fronts emerge inside the MinD wave profil which subsequently annihilate the back part of the MinD wave. This phenomenon resembles the *in vivo* formation of the MinE ring. In cells, a new MinE front forms only after the old MinE front has disappeared at one cell pole, i.e. when the MinE solution concentration is temporarily increased.

Finally we could under certain conditions observe the transition of Min waves to more complex spatiotemporal patterns when increasing the viscosity and crowd-

ing of the buffer. These patterns were functional in the sense that the system could switch back to wave patterns again. It is not clear if they are a transient phenomenon or if they are a stable regime. Chaotic patterns and chemical turbulence are common phenomena in reaction diffusion systems. We are not aware however that such patterns have been reported for the Min system.

Outlook

The solution in the flow channel can be exchanged within a few seconds. This should make the setup suitable to determine membrane binding rates with a stopped flow experiment. The flow cell is quickly incubated with the protein solution and then a time series of the fluorescence intensity on the membrane is acquired. This type of experiment gives adsorption and desorption rates at the same time. It would be interesting to have more detailed reaction kinetics for the Min system, i.e. to determine k_{on} and k_{off} rates for the membrane binding of MinD and MinE alone and when both are interacting. This might further elucidate how important effects such as cooperativity of MinD or persistent binding of MinE actually are for the formation of Min waves. For examples, it has been questioned why the shape of the MinE profile in Min waves is qualitatively different from the profile of MinD. The concentration of MinE basically increases linearly along the wave profile whereas the MinD profile shows a strong boost in the beginning.

However all theoretical models predict so far that the MinE profile should be similar to MinD. These models assume that MinE binds directly to MinD on the membrane. On the other side, it is possible that MinE binds first to the membrane and only then forms a complex with MinD. A solution NMR study of MinE from *N. gonorrhoeae* showed that the MinD binding domain of MinE is rather unexposed in solution but that MinE can undergo conformational changes [50]. Thus membrane binding of MinE could be the rate limiting step in the formation of the membrane bound MinDE complex. This would explain the linearity of the MinE profile. However to answer such questions on the mechanism one would

need to compare k_{off} values for MinE attachment to the membrane in absence and in presence of MinD.

Detailed kinetics might also clarify the molecular origin of MinD cooperativity and which constants influence the wave length of the Min oscillator. A previous study on Min proteins has shown that k_{on} and k_{off} rates can in principle be determined by single-molecule TIRF spectroscopy [44]. This would be an alternative to the stopped flow experiment in the flow cell setup

The Min system illustrates again the importance of cooperativity and multivalent binding for the emergence of dynamic molecular self-organization. MinD monomers seem to have a very weak affinity for membranes. By doubling or oligomerizing they drastically increase their membrane affinity. MinE homodimers have a rather weak membrane affinity and do not bind to MinD-ATP in solution. However if a membrane and MinD are in close neighborhood, MinE forms a rather stable complex with both [45]. We would expect that cooperativity also plays an important role in the mechanism of other self-organizing systems in bacteria. The concept of cooperativity was also applied in synthetic systems [51, 52].

5 Methods

5.1 Preparation of liposomes

E. coli polar lipid extracts in chloroforme were purchased from Avanti Polar Lipids Inc. (Alabaster, AL). Small unilamellar vesicles and lipid bilayers were produced by essentially following the protocol in [33]. The lipids were dried under a nitrogen flow and placed in a vacuum for 30 min. Subsequently, the dried lipids were dissolved in buffer A ($25\,mM\ Tris-HCl$ pH 7.5, $150\,mM\ KCl$, $5\,mM\ MgCl_2$) and incubated at 37°C for $30\,min$. This gives rise to swelling of the lipid layers on the glass surface and a lipid suspension is formed containing multilamellar vesicles. The suspension was then sonicated in a water bath for about $1\,min$ until the suspension clarified and became transparent. Multilamellar vesicles are

destroyed during sonication which gives rise to small unilamellar vesicles (with diameter around 100 nm). The SUVs were stored at -20°C before further usage.

5.2 Polydimethylsiloxane (PDMS) coated glass cover slips

As support for our lipid bilayers we typically used PDMS coated glass cover slips (150 μm thickness). The thin PDMS layer was produced as follows:

A silica wafer (10 cm diameter) was first coated with a trimethylsilyl layer by incubating it for 30 min in a $(CH_3)_3SiCl$ atmosphere. 15 g PDMS (Sylgard 184, Dow Corning) was mixed with the crosslinker at a 9 : 1 mass ratio, degased in vacuum and poured on top of the silica wafer. The glass cover slips were then pressed on the PDMS covered wafer. After curing the PDMS overnight at 70°C, the PDMS coated glass cover slips were carefully peeled off the wafer and stored at room temperature until further usage. The PDMS mold typically had a thicknes of around 50 μm.

5.3 Preparation of supported lipid bilayers

Supported lipid bilayers were formed by vesicle fusion of SUVs. The PDMS support was first plasmacleaned for 5 min to make it more hydrophylic. The flow channel was glued on the PDMS support and exposed for 10 min to a UV lamp to cure the UV glue (Norland optical adhesive 63). We next attached silicon tubes to the flow channel. Using a syringe a liposome solution was applied to the PDMS support at a concentration of 0.25 mg/ml. We added 2.5 mM of $CaCl_2$ to enhance vesicle rupture. The vesicles were incubated for 10 min at 37°C forming a lipid bilayer on the PDMS support. Using two syringes the bilayer was subsequently washed three times with 1 ml of buffer A.

5.4 Construction of the flow cell

The flow chamber was designed using the freely available software Sketchup 8. Alternatively commcercially available softwares such as AutoCAD or Solidworks

could be used. The Sketchup model was exported as an STL file. We next used the software netfabb to check if the generated STL can be further processed. But this step is optional. The STL file was then printed with the Ultimaker 3D printer. Polylactic acid (PLA) was used as a printing material which is a hydrophobe polymer that is stable towards aqueous solutions. In our experiments we typically used flow channels of the following size: the diameter of the entrance hole is 3 mm. This hole size is compatible with the 3 mm diameter of the silicon tubes that were attached to the channel. The whole construct had a size of 10 mm height, 16 mm length and 6 mm width. The channel inside was 7 mm long, 2 mm wide and 1 mm high. The total volume was 130 μl. A model of the flow channel is shown in section 3.1.

5.5 Min protein incubation

The flow cell was incubated with Min proteins by exchanging the buffer solutions with a syringe. Regular Min waves usually had formed after 2 h.

5.6 Live imaging of the flow cell

When we wanted to image the lipid bilayer in the flow chamber while exchanging the buffer solution we attached the flow channel to a low pressure syringe pump (cetoni neMESYS). We used teflon hoses to connect the syringe in the pump to the flow channel. Teflon hoses seemed to produce considerably less artefacts than silicon hoses. An experiment of the type "incubate solution 1 for 2h and exchange it by solution 2" was done as follows: Directly after inserting solution 1 into the flow channel we attached the teflon hose with solution 2 to the flow channel. We then waited until the incubation of the Min proteins was finished inside the flow channel and exchanged the two solutions while simultaneously imaging with microscope. A photo of the experimental setup is shown in Fig. 5.1. Connecting the whole system already in the beginning worked more reliable. For example one avoids the insertion of air bubbles during the experiment.

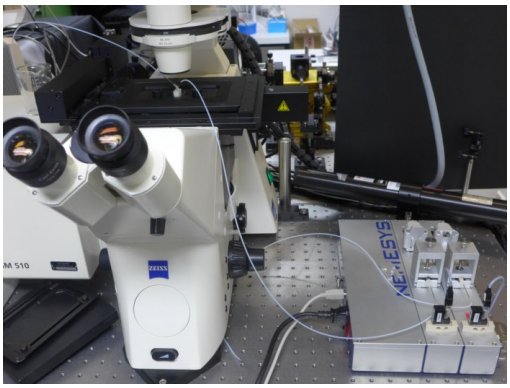

Figure 5.1: The image shows the flow cell being attached simultaneously to a syringe pump and to the sample holder of the confocal microscope.

5.7 Confocal Laser Scanning Microscopy

Confocal Laser Scanning Microscopy is an experimental method that combines fluorescence laser spectroscopy with a confocal setup. It permits the construction of 3D images of the specimen and compared to widefield light microscopes it produces sharper images with higher contrast up to the diffraction limit [53]. We used a LSM780 and a LSM510 Zeiss microscope to acquire the microscope images shown in this work.

5.8 Fluorescence Recovery after Photobleaching (FRAP)

Fluorescence recovery after photobleaching is a method to determine diffusion coefficients and binding constants of fluorescently labelled compounds. It has traditionally been used in the context lipid bilayers but has also found applications in determining in vivo solution kinetics [54]. The fluorophore in a small circular region of the membrane is bleached by exposing it to high laser intensity during a short time. Due to diffusion or other transport processes the photobleached fluorophores move out of the bleached area and new fluorescent particles diffuse into it. This leads to fluorescence recovery in the observed region. Quantitative information about diffusion coefficients can be obtained by recording a time series of the observed region and fitting an appropriate function to it.

Certain theoretical models of fluorescence recovery can be solved analytically, in particular when only membrane diffusion of the fluorophore is present and a circular area of radius r is bleached [55, 56]. In this case the fluorescence recovery $F(t)$ at the center of the bleached circle follows the equation [57]

$$F_0 - F(t) = A\left(1 - \exp\left(-\frac{r^2}{4Dt}\right)\right) + B \tag{5.1}$$

where F_0 is the fluorescence intensity before bleaching, D the diffusion constant and A, B constants corresponding to the mobile and immobile fraction of lipids in the membrane. The diffusion coefficient for each measurement was calculated by fitting (5.1) to the experimental FRAP curves. The data was analysed using OriginPro.

Image analysis

Microscope images were analysed using ImageJ [58].

Acknowledgements

The present work was carried out in the research group of Prof. Petra Schwille at the Max Planck Institute for Biochemistry in Martinsried. A number of people supported me during the time of my work.

Petra Schwille gave me the opportunity to do the research stay in her lab with an excellent and international working environment.

Damien Baigl sacrified a lot of his time for discussing my project.

I am especially thankful to Katja Zieske who supervised my internship and who took a lot of her time throughout my stay to introduce me to new experimental techniques and to discuss my project. Helge Vogl helped me with the construction of the flow cell. Philipp Blumhardt kindly agreed to review this manuscript. Matías Hernández introduced me to weightlifting. I would like to thank Simon Kretschmer, Ariadna Martos Sanchez, Henri Franquelime, Zdenek Petrasek and all the other members of the group for continuous discussions about Min proteins and membranes in general - it was a pleasure to work in this group.

I would like to thank my family for their continuous support.

References

[1] Wickstead, B.; Gull, K. *J. Cell Biol.* **2011**, *194*, 513–25.

[2] Shih, Y.-L.; Rothfield, L. *Microbiol. Mol. Biol. Rev.* **2006**, *70*, 729–54.

[3] Jones, L. J.; Carballido-López, R.; Errington, J. *Cell* **2001**, *104*, 913–22.

[4] Kiekebusch, D.; Thanbichler, M. *Trends Microbiol.* **2014**, *22*, 65–73.

[5] Shapiro, L.; McAdams, H. H.; Losick, R. *Science* **2009**, *326*, 1225–8.

[6] Marston, a. L.; Thomaides, H. B.; Edwards, D. H.; Sharpe, M. E.; Errington, J. *Genes Dev.* **1998**, *12*, 3419–3430.

[7] Hwang, L. C.; Vecchiarelli, A. G.; Han, Y.-W.; Mizuuchi, M.; Harada, Y.; Funnell, B. E.; Mizuuchi, K. *EMBO J.* **2013**, *32*, 1238–49.

[8] Savage, D. F.; Afonso, B.; Chen, A. H.; Silver, P. a. *Science* **2010**, *327*, 1258–61.

[9] Turing, A. M. *Philos. Trans. R. Soc. B Biol. Sci.* **1952**, *237*, 37–72.

[10] Nicolis, G.; Prigogine, I. *Self-organization in nonequilibrium systems: from dissipative structures to order through fluctuations*; A Wiley-Interscience Publication; Wiley, 1977.

[11] Zhdanov, V. P. *Surf. Sci. Rep.* **2002**, *45*, 231–326.

[12] Imbihl, R.; Ertl, G. *Chem. Rev.* **1995**, *95*, 697–733.

[13] Raskin, D. M.; de Boer, P. a. *Proc. Natl. Acad. Sci. U. S. A.* **1999**, *96*, 4971–6.

[14] Raskin, D. M.; de Boer, P. A. *J. Bacteriol.* **1999**, *181*, 6419–24.

[15] Hale, C. a.; Meinhardt, H.; de Boer, P. a. *EMBO J.* **2001**, *20*, 1563–72.

[16] Arumugam, S.; Petrašek, Z.; Schwille, P. *Proc. Natl. Acad. Sci. U. S. A.* **2014**, *111*, E1192–200.

[17] Hu, Z.; Lutkenhaus, J. *J. Bacteriol.* **2000**, *182*, 3965–71.

[18] Bisicchia, P.; Arumugam, S.; Schwille, P.; Sherratt, D. *MBio* **2013**, *4*, e00856–13.

[19] Martos, A.; Jiménez, M.; Rivas, G.; Schwille, P. *Trends Cell Biol.* **2012**, *22*, 634–43.

[20] Forster, A. C.; Church, G. M. *Mol. Syst. Biol.* **2006**, *2*, 45.

[21] Loose, M.; Fischer-Friedrich, E.; Ries, J.; Kruse, K.; Schwille, P. *Science* **2008**, *320*, 789–92.

[22] Rothfield, L.; Justice, S.; García-Lara, J. *Annu. Rev. Genet.* **1999**, *33*, 423–48.

[23] Donachie, W. D. *Annu. Rev. Microbiol.* **1993**, *47*, 199–230.

[24] Harry, E.; Monahan, L.; Thompson, L. *Int. Rev. Cytol.* **2006**, *253*, 27–94.

[25] Löwe, J.; Amos, L. a. *Nature* **1998**, *391*, 203–6.

[26] Bi, E. F.; Lutkenhaus, J. *Nature* **1991**, *354*, 161–4.

[27] Errington, J.; Daniel, R. A.; Scheffers, D.-J. *Microbiol. Mol. Biol. Rev.* **2003**, *67*, 52–65.

[28] Lutkenhaus, J.; Pichoff, S.; Du, S. *Cytoskeleton (Hoboken).* **2012**, *69*, 778–90.

[29] Adams, D. W.; Errington, J. *Nat. Rev. Microbiol.* **2009**, *7*, 642–53.

[30] Ma, X.; Ehrhardt, D. W.; Margolin, W. *Proc. Natl. Acad. Sci. U. S. A.* **1996**, *93*, 12998–3003.

[31] Männik, J.; Wu, F.; Hol, F. J. H.; Bisicchia, P.; Sherratt, D. J.; Keymer, J. E.; Dekker, C. *Proc. Natl. Acad. Sci. U. S. A.* **2012**, *109*, 6957–62.

[32] Loose, M.; Kruse, K.; Schwille, P. *Annu. Rev. Biophys.* **2011**, *40*, 315–36.

[33] Zieske, K.; Schwille, P. *Angew. Chem. Int. Ed. Engl.* **2013**, *52*, 459–62.

[34] Halatek, J.; Frey, E. *Cell Rep.* **2012**, *1*, 741–52.

[35] Bonny, M.; Fischer-Friedrich, E.; Loose, M.; Schwille, P.; Kruse, K. *PLoS Comput. Biol.* **2013**, *9*, e1003347.

[36] Martos, A.; Petrasek, Z.; Schwille, P. *Environ. Microbiol.* **2013**, *15*, 3319–26.

[37] Michie, K. a.; Löwe, J. *Annu. Rev. Biochem.* **2006**, *75*, 467–92.

[38] Lutkenhaus, J. *Annu. Rev. Biochem.* **2007**, *76*, 539–62.

[39] Wu, W.; Park, K.-T.; Holyoak, T.; Lutkenhaus, J. *Mol. Microbiol.* **2011**, *79*, 1515–28.

[40] Boer, P. D.; Crossley, R. *EMBO J* **1991**, *1*, 4371–4380.

[41] Lackner, L. L.; Raskin, D. M.; de Boer, P. A. J. *J. Bacteriol.* **2003**, *185*, 735–49.

[42] Renner, L. D.; Weibel, D. B. *J. Biol. Chem.* **2012**, *287*, 38835–44.

[43] Hu, Z.; Gogol, E. P.; Lutkenhaus, J. *Proc. Natl. Acad. Sci. U. S. A.* **2002**, *99*, 6761–6.

[44] Loose, M.; Fischer-Friedrich, E.; Herold, C.; Kruse, K.; Schwille, P. *Nat. Struct. Mol. Biol.* **2011**, *18*, 577–83.

[45] Park, K.-T.; Wu, W.; Battaile, K. P.; Lovell, S.; Holyoak, T.; Lutkenhaus, J. *Cell* **2011**, *146*, 396–407.

[46] Chebotareva, N. a.; Kurganov, B. I.; Livanova, N. B. *Biochem. BiokhimiiÍ¡a* **2004**, *69*, 1239–51.

[47] Mikhailov, A. S.; Showalter, K. *Phys. Rep.* **2006**, *425*, 79–194.

[48] Kuramoto, Y. *Prog. Theor. Phys.* **1980**, *63*, 1885–1903.

[49] Ivanov, V.; Mizuuchi, K. *Proc. Natl. Acad. Sci.* **2010**, *107*, 8071–8078.

[50] Ghasriani, H.; Ducat, T.; Hart, C. T.; Hafizi, F.; Chang, N.; Al-Baldawi, A.; Ayed, S. H.; Lundström, P.; Dillon, J.-A. R.; Goto, N. K. *Proc. Natl. Acad. Sci. U. S. A.* **2010**, *107*, 18416–21.

[51] Fasting, C.; Schalley, C. a.; Weber, M.; Seitz, O.; Hecht, S.; Koksch, B.; Dernedde, J.; Graf, C.; Knapp, E.-W.; Haag, R. *Angew. Chem. Int. Ed. Engl.* **2012**, *51*, 10472–98.

[52] Albertazzi, L.; Martinez-Veracoechea, F. J.; Leenders, C. M. a.; Voets, I. K.; Frenkel, D.; Meijer, E. W. *Proc. Natl. Acad. Sci. U. S. A.* **2013**, *110*, 12203–8.

[53] Pawley, J. In *Handbook Of Biological Confocal Microscopy*, 3rd ed.; Pawley, J. B., Ed.; Springer US: Boston, MA, 2006.

[54] Sprague, B. L.; McNally, J. G. *Trends Cell Biol.* **2005**, *15*, 84–91.

[55] Axelrod, D.; Koppel, D. E.; Schlessinger, J.; Elson, E.; Webb, W. W. *Biophys. J.* **1976**, *16*, 1055–69.

[56] Soumpasis, D. M. *Biophys. J.* **1983**, *41*, 95–7.

[57] Kapitza, H. G.; McGregor, G.; Jacobson, K. A. *Proc. Natl. Acad. Sci. U. S. A.* **1985**, *82*, 4122–6.

[58] Schneider, C. a.; Rasband, W. S.; Eliceiri, K. W. *Nat. Methods* **2012**, *9*, 671–675.